Supporting Information

Iron-doped nickel sulfide @ phosphate heterostructures nanosheets constructed by hydrothermal P_2S_5 and layered double hydroxides for electrocatalytic oxygen evolution

Zeyi Wang [a], Shuling Liu [a] *, Chenglong Wang [b], Dan Ren [b], Yanling Hu [a], Yujie Ma [a], Chao Wang [a] *

[a] *Department of Chemistry and Chemical Engineering, The Youth Innovation Team of Shaanxi Universities, Shaanxi University of Science and Technology, Xi'an, Shaanxi 710021, China*

[b] *School of Chemical Engineering and Technology, Xi'an Jiaotong University, West Xianning Road 28, Xi'an 710049, PR China*

* Corresponding author:

E-mail address: shulingliu@aliyun.com

cwang@sust.edu.cn

Content：

1. Experimental

Chemicals

Nickel (II) nitrate hexahydrate ($Ni(NO_3)_2·6H_2O$; Guanghua Chemical Reagent; AR 98.0%), potassium hydroxide (KOH; Kermel Chemical Reagent; AR 85.0%), Phosphorus pentasulfide (P_2S_5; Fuchen Chemical Reagent; AR), ethanol (C_2H_5OH;Rionlon Chemical Reagent; AR 99.7%), N, N-dimethylformamide (C_3H_7NO; Fuyu chemical ; reagent AR 99.5%)) benzene (C_6H_6; Hushi Chemical Reagent; AR 99.5%),methanol (CH_3OH; Guanghua Chemical Reagent; AR 99.5%), hydrochloric acid (HCl; Kelong Chemical Reagent; AR 38%),ferrous sulfate heptahydrate ($FeSO_4·7H_2O$; Tianli Chemical Reagent; AR 99.0%), Ammonium fluoride (NH_4F; Oberkai chemical reagent; AR 99.0%),sodium sulfate anhydrous (Na_2SO_4; Damao Chemical Reagent; AR 99.0%), potassium nitrate (KNO_3; Hengxing Chemical Reagent; AR 99.0%), urea (H_2NCONH_2 Damao Chemical Reagent; AR 99.0%), tetramethylammonium hydroxide pentahydrate ($C_4H_{13}NO·5H_2O$; Macklin Chemical Reagent; AR 97.0%), Ni foam (thickness 1.5 mm) were used as received unless stated otherwise. Doubly distilled water was used throughout the experiment.

Prior to experiments, NF (3×2 cm^2) were ultrasonically cleaned in hydrochloric acid (0.1 M), acetone and ethanol consecutively for 10 min each to remove contaminants and surface oxides, then rinsed with deionized water, dried in oven and stored for subsequent use.

Preparation of $Ni(OH)_2$/NF

$Ni(NO_3)_2 \cdot 6H_2O$ (0.727g), NH_4F (0.37g) and urea (1.5g) were mixed in 30 mL of water. The resulting solution was poured into a 50 ml Teflon-lined autoclave with a piece of 3 × 2 cm^{-2} cleaned NF. The hydrothermal process was carried out at 120 ℃ in an electric oven for 6 h. After natural cooling to room temperature, the $Ni(OH)_2$ coated on NF was washed with deionized water, then blown dry under a stream of compressed air. The mass of $Ni(OH)_2$ on NF is weighed by a laboratory balance to 5.5 mg cm^{-2}.

Preparation of NiS@$Ni_3(PO_4)_2$/NF

The 30 ml DMF (N, N-dimethylformamide) were added to 50 ml Teflon-lined autoclave, and the prepared $Ni(OH)_2$/NF was into the Teflon-lined autoclave leaning against the wall, with 0.18 mmol phosphorus pentasulfide (P_2S_5) added. The autoclave was kept at 150℃ for 14 h. After natural cooling, the NiS@$Ni_3(PO_4)_2$/NF was removed from the autoclave, washed with ethanol and water, and dried under vacuum at 60 ℃ for 6 h. Crop it to 1 × 2 cm^2 for testing. The mass of NiS@$Ni_3(PO_4)_2$/NF on NF is weighed by a laboratory balance to be 3.0 mg cm^{-2}.

2. Instrumentation

X-ray photoelectron spectroscopy (XPS) was carried out using a Kratos Axis Supra spectrometer at room temperature and ultra-high vacuum (UHV) conditions. The instrument was equipped with monochromatic Al Kα source 1486.6 eV (15 mA, 15 kV), and hemispherical analyser with hybrid magnetic and electrostatic lens for enhanced electron collection. Survey and detailed XPS spectra were acquired at normal emission with the fixed pass energy of 160 eV and 40 eV, respectively. All spectra were charge-corrected to the hydrocarbon peak set to 284.6 eV. The Kratos charge neutralizer system was used on all specimens. Data analysis was based on a standard deconvolution method using mixed Gaussian (G) and Lorentzian (L) line shape (G = 70% and L = 30%, Gaussian - Lorentzian product) for each component. Spectra were analyzed using CasaXPS software (version 2.3.16). X-ray diffraction (XRD) was acquired using (D8 ADVANCE, Bruker) diffractometer having Cu Kα (λ=1.54 A) source. The instrument was operated at 30 mA current voltage and 40 kV. Field emission scanning electron microscope (S-4800, Hitachi, Japan) and transmission electron microscope (FEI-Tecnai G2 F20) were used to observe the morphology of the catalyst. A concentric nebulizer was used with a cyclonic spray chamber.

Electrochemical measurements were carried out using electrochemical workstations (CHI660E and ParSTAT MC). The geometric area of the working electrode immersed in the electrolyte is controlled to 1 cm^2. The Tafel slope (b) is calculated by Eq. S1.

$$\eta = b \log j \qquad \text{(S1)}$$

where η is the overpotential, b is the Tafel slope, and j is the current density. AC

electrochemical impedance spectroscopy (EIS) is performed with the alternating voltage amplitude at 5 mV in the range of 100 kHz to 0.01 Hz. The solution resistance acquired from the EIS is used for *iR* compensation, and all the linear sweep voltammetry and galvanostatic measurements are *iR* compensated. The potentials are reported in reversible hydrogen electrode (RHE) scale unless otherwise stated.

3. X-ray photoelectron spectroscopy

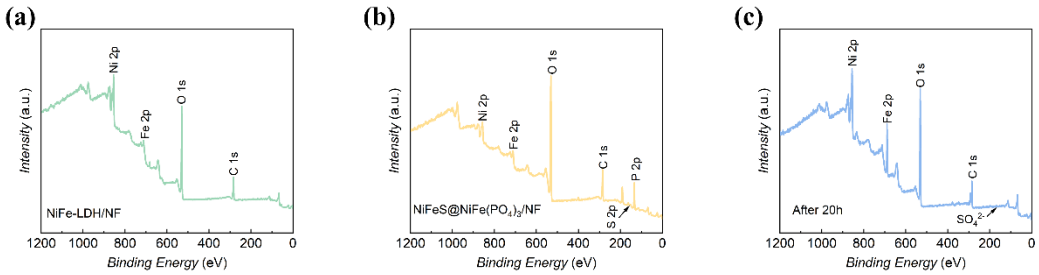

Figure S1. (a) XPS spectra of NiFe-LDH/NF and (b) $Ni_{0.9}Fe_{0.1}S@NiFe(PO_4)_x$/NF and (c) $Ni_{0.9}Fe_{0.1}S@NiFe(PO_4)_x$/NF after 22 h OER test.

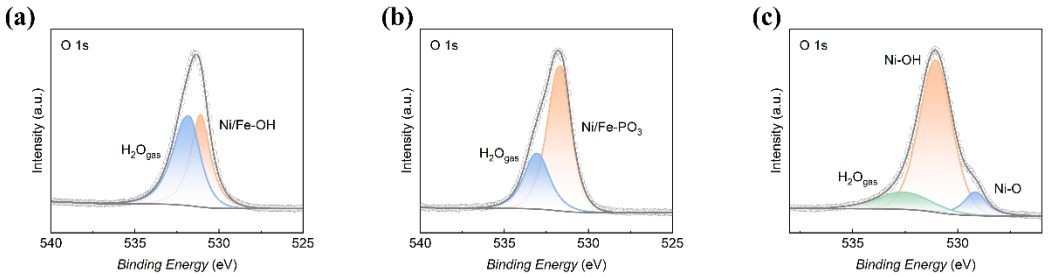

Figure S2. (a) O 1s XPS spectra of NiFe-LDH/NF and (b) $Ni_{0.9}Fe_{0.1}S@NiFe(PO_4)_x$/NF and (c) $Ni_{0.9}Fe_{0.1}S@NiFe(PO_4)_x$/NF after 22 h OER test.

4. Raman spectra

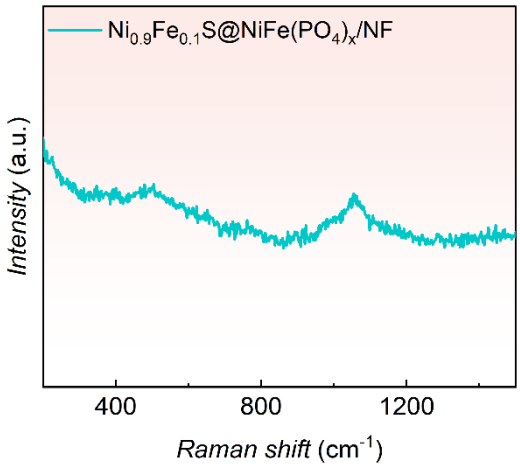

Figure S3. Raman spectra of the $Ni_{0.9}Fe_{0.1}S@NiFe(PO_4)_x$/NF.

5. Electrochemistry

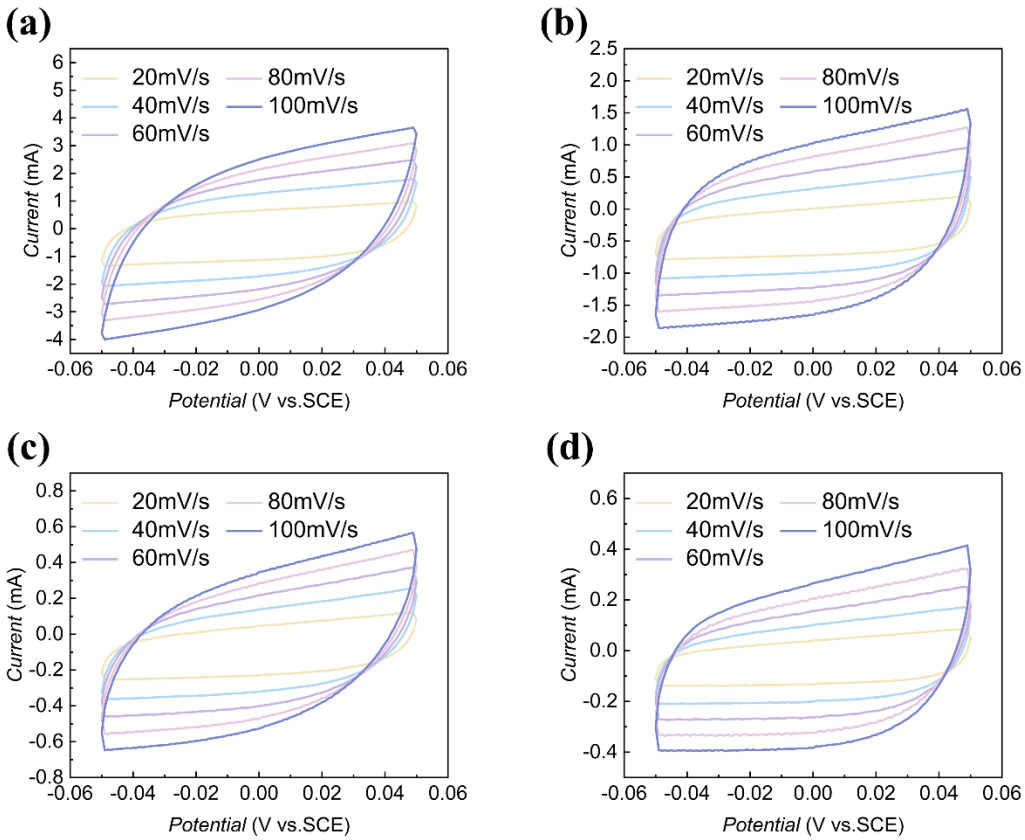

Figure S4. (a-d) CV of NiS@$Ni_3(PO_4)_2$/NF, $Ni_{0.9}Fe_{0.1}S$@NiFe$(PO_4)_x$/NF, NiFe-LDH/NF and Bare NF at different scan rates (20, 40, 60, 80, and 100 mV s^{-1}) in -0.05 - 0.05 V in 1 M KOH.

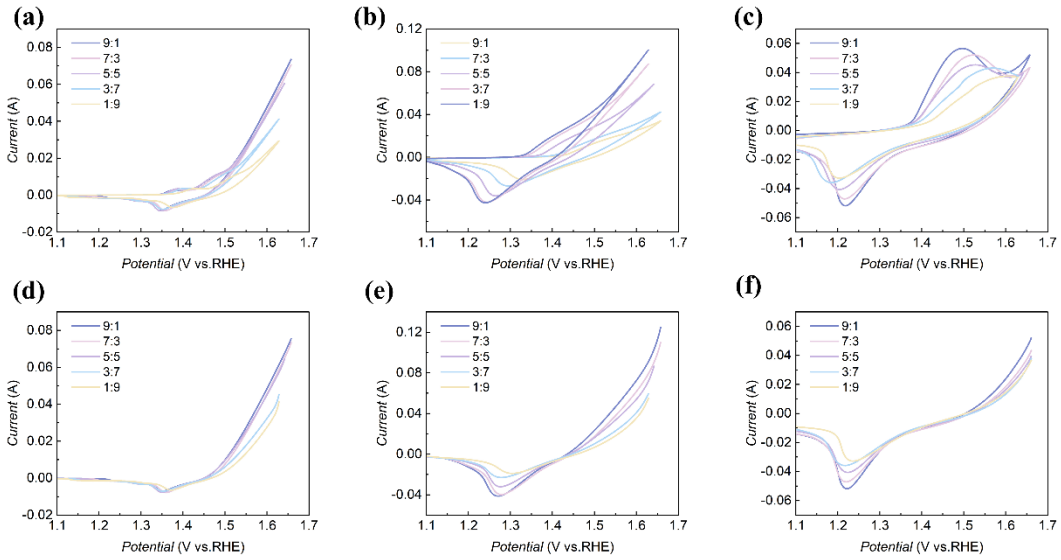

Figure S5. The CV and LSV of the (a, d) NiFe-LDH/NF; (b, e) $Ni_{0.9}Fe_{0.1}S@NiFe(PO_4)_x$/NF and (c,f) $NiS@Ni_3(PO_4)_2$/NF in different pH solutions (x M KOH + (1-x) M KNO_3, pH=13.84, 13.72, 13.57, 13.35, and 12.9) at scan rate 5 mV s^{-1}.

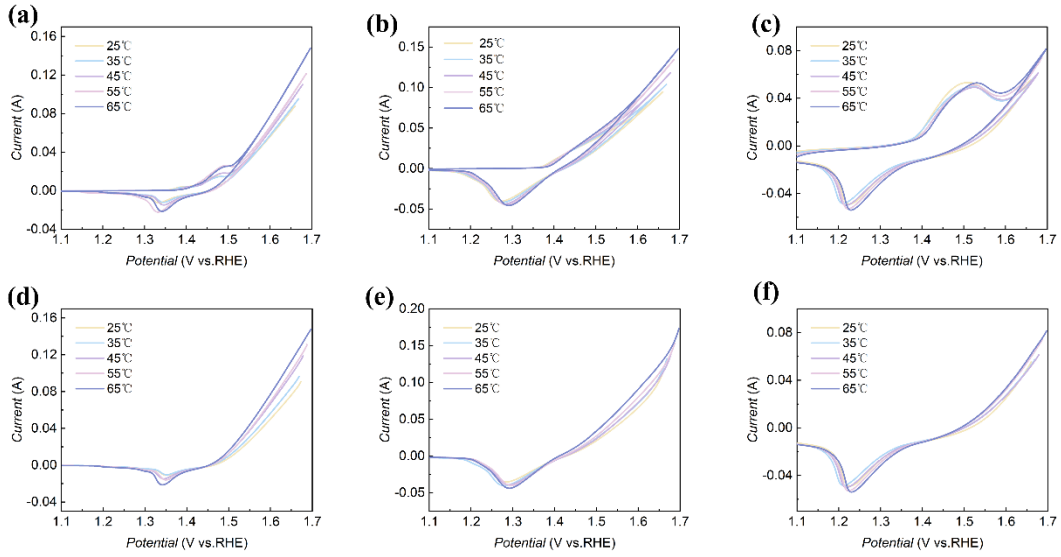

Figure S6. The CV and LSV of the (a, d) NiFe-LDH/NF and (b, e) $Ni_{0.9}Fe_{0.1}S@NiFe(PO_4)_x$/NF and (c f) $NiS@Ni_3(PO_4)_2$/NF at different temperatures in 1 M KOH at scan rate 5 mV s^{-1}.

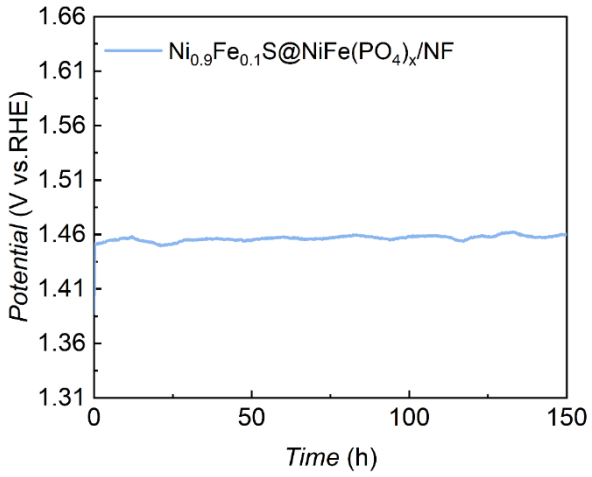

Figure S7. The time potential curve of the catalyst $Ni_{0.9}Fe_{0.1}S@NiFe(PO_4)_x/NF$ with a constant current density of 10mA cm^{-2} was obtained at 1M KOH for about 150 h.

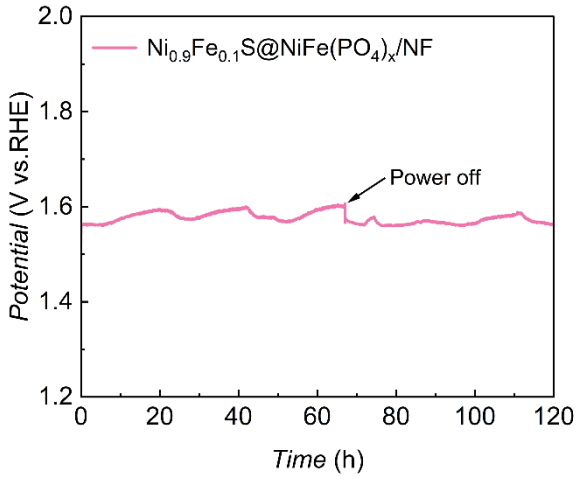

Figure S8. The time potential curve of the catalyst $Ni_{0.9}Fe_{0.1}S@NiFe(PO_4)_x/NF$ with a constant current density of 100mA cm^{-2} was obtained at 1M KOH for about 120 h.

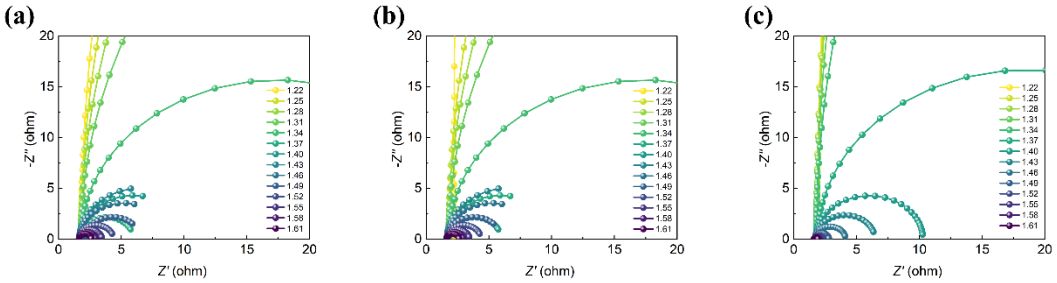

Figure S9. Nyquist plots of the NiFe-LDH/NF (a), NiS@$Ni_3(PO_4)_2$/NF (b) and $Ni_{0.9}Fe_{0.1}S$@$NiFe(PO_4)_x$/NF (c) at different potentials.

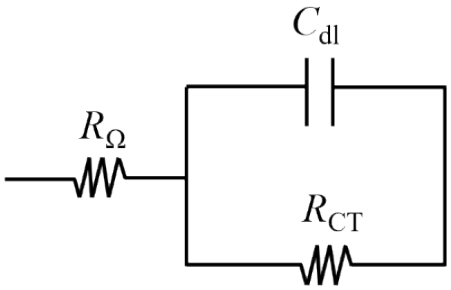

Figure S10. The equivalent circuit used for fitting EIS spectra to acquire R_{ct}.

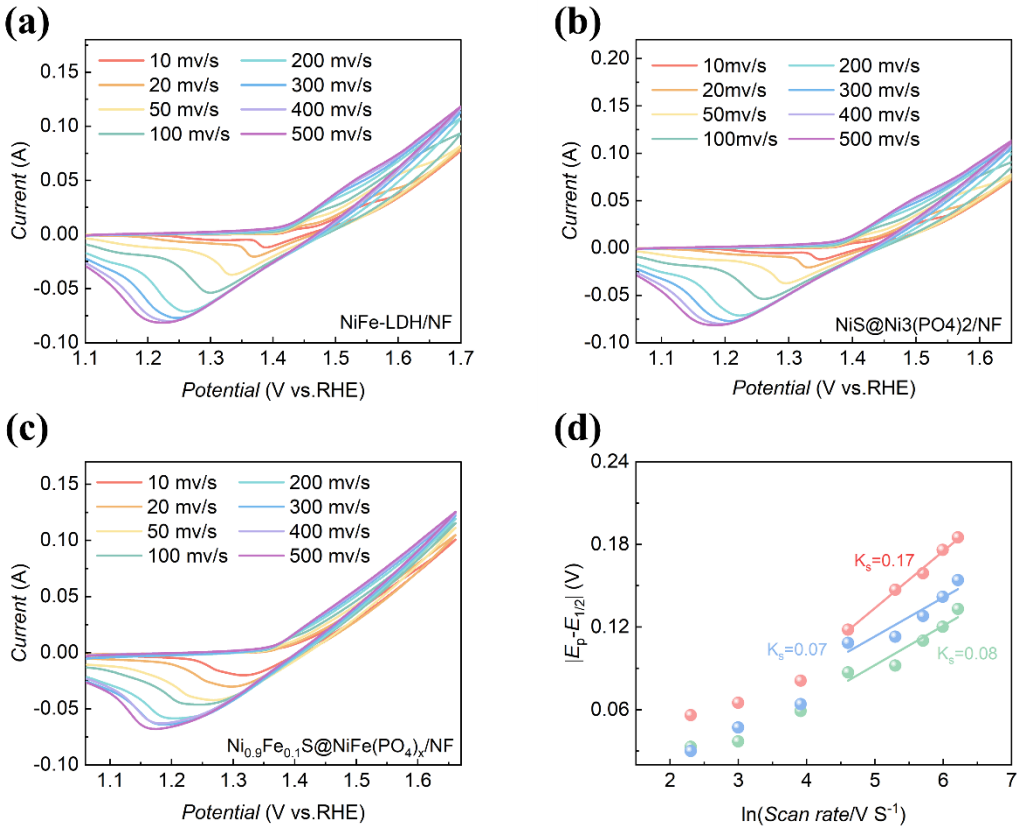

Figure. S11. CV of NiFe-LDH/NF (a) $NiS@Ni_3(PO_4)_2/NF$ (b) and $Ni_{0.9}Fe_{0.1}S@NiFe(PO_4)_x/NF$ (c) at different scan rates (10-500 mV s-1) in 1 M KOH; (d) *K*s of NiFe-LDH/NF,$NiS@Ni_3(PO_4)_2/NF$ and $Ni_{0.9}Fe_{0.1}S@NiFe(PO_4)_x/NF$ obtained from a Laviron analysis.

Fig. S11 a-c shows the CV of NiFe-LDH/NF, $NiS@Ni_3(PO_4)_2/NF$ and $NiFeS@Ni_3Fe(PO_4)_3/NF$ under different conditions The scanning rate. The electron transfer rate constant (k) is determined by Laviron Equation[1, 2] (Eq. S2)

$$E_c = E_{1/2} - (RT/\alpha nF)\ln(\alpha nF/RTK_s) - (RT/\alpha nF)\ln(v) \quad (S2)$$

where E_c is the reduction potential of metal redox, $E_{1/2}$ is the formal potential of metal redox, R is the universal gas constant, T is the temperature in kelvin, n is the number of electrons transferred, a is the transfer coefficient, k_s is the rate constant of

metal redox, and v is the scan rate in the CV measurements.

The turnover frequency (*TOF*) was calculated as follows (Eq. S3):

$$TOF = j \cdot N_A / n \cdot F \cdot \Gamma \qquad \text{(S3)}$$

where j is the current density, N_A is the Avogadro number, n is the number of electron transferred for the evolution of a single O_2 molecule, F is the Faraday constant, and Γ is the surface concentration or the number of active Ni sites.

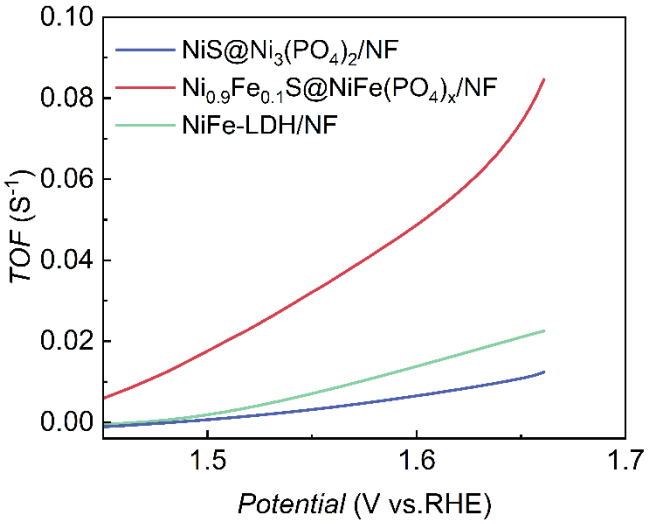

Figure. S12. TOF values against the applied potential in the OER region.

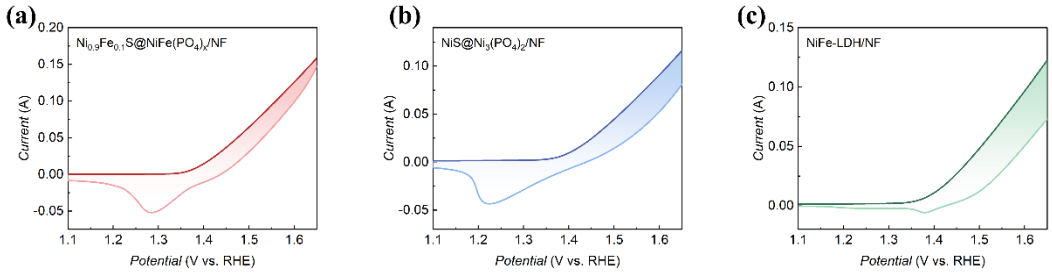

Figure. S13. LSV curves of (a) $Ni_{0.9}Fe_{0.1}S@NiFe(PO_4)_x/NF$, (b) $NiS@Ni_3(PO_4)_2/NF$ and (c) NiFe-LDH/NF in 1 M KOH electrolyte (light color) and 1 M KOH with extra MeOH (dark color).

6. EDS

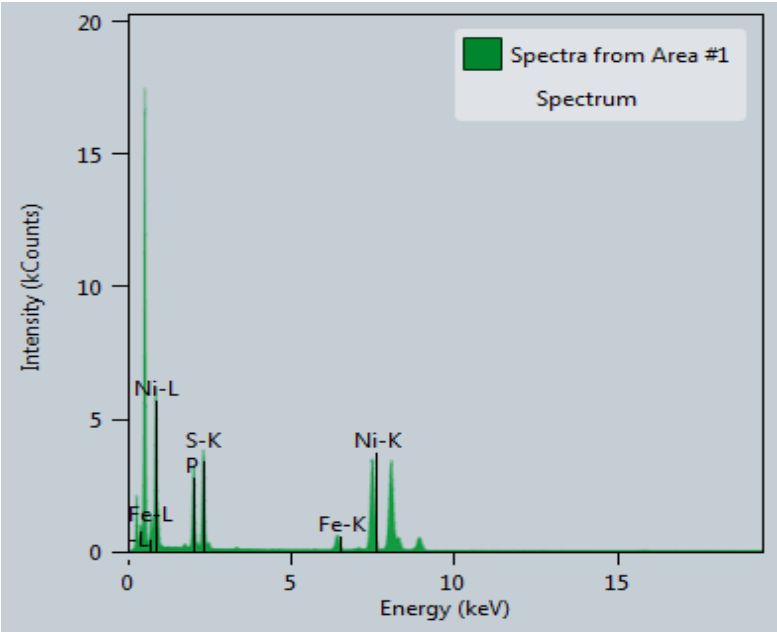

Figure S14. EDS spectrum obtained for $Ni_{0.9}Fe_{0.1}S@NiFe(PO_4)_x$ on NF.

Table S1. Contents of the deposited films

		Atomic Percentage (%)			
		Ni	Fe	S	P
NiFe-LDH	XPS	90.72	9.28	-	-
$Ni_{0.9}Fe_{0.1}S$@$NiFe(PO_4)_x$/NF	XPS	36.9	3.44	41.85	17.81
	EDS	50.73	6.84	23.5	18.93
	ICP-MS	59.76	6.64	22.48	11.12
Post 20h OER	XPS	65.61	4.11	30.28	-

Table S2. EIS fitting results

	R_s / Ω	Error / %	R_{ct} / Ω	Error / %
NiS@$Ni_3(PO_4)_2$/NF	1.641	0.21463	1.78	1.68
NiFe-LDH/NF	1.681	0.4643	1.13	1.34
$Ni_{0.9}Fe_{0.1}S$@$NiFe(PO_4)_x$/NF	1.631	0.21432	0.48	0.98
Bare NF	25.26	1.1268	56.53	3.22

7. SEM

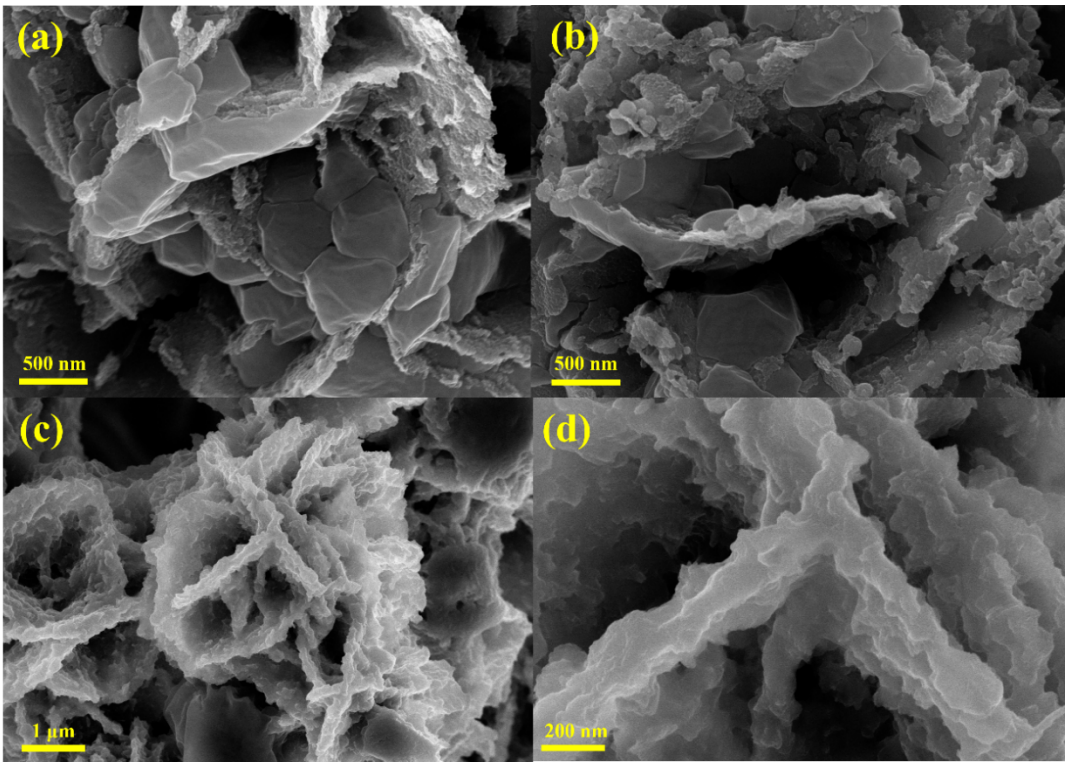

Figure S15. SEM images of (a-b) $Ni_{0.9}Fe_{0.1}S@NiFe(PO_4)_x/NF$ (c-d) $Ni_{0.9}Fe_{0.1}S@NiFe(PO_4)_x/NF$ after the long-term galvanostatic OER test.

8. TEM

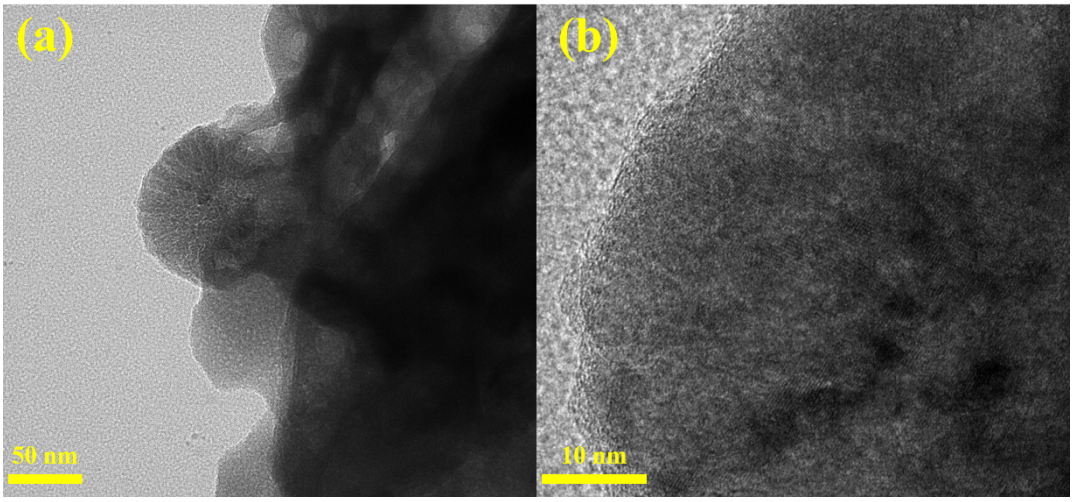

Figure S16. (a) TEM and (b) HRTEM images of $Ni_{0.9}Fe_{0.1}S$@$NiFe(PO_4)_x$/NF.

9. Activity comparison

Table S3. OER activity comparison in alkaline solutions

Catalysts	η at 10 mA cm^{-2} / mV	*Tafel slope* / mV dec^{-1}	Stability / h	References
NiFeS@$Ni_3Fe(PO_4)_3$/NF	208	38.75	150	This work
Fe-(NiP_2/Ni_2P)/CNT	254	46.1	20	3
NiFeP@NiP/NF	227	60.7	120	4
NiFeP	265	40.9	20	5
NiP_2/FeP/CNT	261	44.0	20	6
$Ni_{0.85}Fe_{0.15}$PS/NF	251	34.0	50	7
NiFe-P NiFe-P	233	42.5	30	8
NiFe$(OH)_x$/NiP_x/NF	220	35	18	9
CoOOH/SO_4^{2-}/NiOOH	250	56	100	10
$CuFeS_2$-BM	243	77.21	24	11
Ni-CoS/NC	270	37	300	12
(Ni,Fe)S_2/NiFe-CNFs	287@30mA	52.06	48	13
NiCoS/FeO@CC	190	45	25	14
$CoNi_5S_8$-Ni_2P-FeP_2	215	34	60	15

Table S4. OER activity comparison in 30wt% KOH solutions

Catalysts	Current density (mA)	Potential (V)	References
$Ni_{0.9}Fe_{0.1}S$@NiFe$(PO_4)_x$/NF	100	1.68	This work
Ni_2P@$FePO_xH_y$	1000	1.71	16
Fe-18h/NF	100	1.69	17
$CuCo_2B$	100	1.5	18
Co-Fe-S NFs@MS/NF	500	1.51	19
$Fe_{11.8\%}$-Ni_3S_2/NF	1000	1.45	20
VN/ CNT/IF	1000	1.64	21
Ni-Fe-Mo	10	1.54	22
Fe-a,b-Ni$(OH)_2$	100	1.46	23
Ni_3Fe-FeV_2O_4@C/NF	10	1.51	24
$(Ni_{0.83}Fe_{0.17})_2P$/NF	100	1.68	25

10.References

1. X. Liu, J. Wang, H. Liao, J. Chen, S. Zhang, L. Tan, X. Zheng, D. Chu, P. Tan and J. Pan, *Nano Letters*, 2023, **23**, 5027-5034.
2. J. Wang, L. Gan, W. Zhang, Y. Peng, H. Yu, Q. Yan, X. Xia and X. Wang, *Science advances*, 2018, **4**, eaap7970.
3. Y. Liu, B. Wang, K. Srinivas, M. Wang, Z. Chen, Z. Su, D. Liu, Y. Li, S. Wang and Y. Chen, *International Journal of Hydrogen Energy*, 2022, **47**, 12903-12913.
4. F. Diao, W. Huang, G. Ctistis, H. Wackerbarth, Y. Yang, P. Si, J. Zhang, X. Xiao and C. Engelbrekt, *ACS Applied Materials & Interfaces*, 2021, **13**, 23702-23713.
5. T. Wang, X.-Z. Fu, S. J. G. E. Wang and Environment, 2022, **7**, 365-371.
6. Y. Liu, B. Wang, Y. Lu, Z. Su, Y. Li, Q. Wu, D. Yang, Y. Chen and S. Wang, *Journal of Materials Science*, 2021, **56**, 16000-16009.
7. W. Peng, J. Li, K. Shen, L. Zheng, H. Tang, Y. Gong, J. Zhou, N. Chen, S. Zhao and M. J. J. o. M. C. A. Chen, 2020, **8**, 23580-23589.
8. P. Li and H. C. J. J. o. M. C. A. Zeng, 2018, **6**, 2231-2238.
9. P. Wang, T. Yu, L. Hao and X. J. J. o. P. S. Liu, 2024, **589**, 233749.
10. Z.-B. Yu, Z. Song, P. Zheng, J. Sun and Z. Yang, *Journal of Physics and Chemistry of Solids*, 2024, **187**, 111862.
11. Z. Chen, R. Zheng, W. Wei, W. Wei, B.-J. Ni and H. Chen, *Journal of Energy Chemistry*, 2022, **68**, 275-283.
12. K. Wan, J. Luo, W. Liu, T. Zhang, J. Arbiol, X. Zhang, P. Subramanian, Z. Fu and J. Fransaer, *Chinese Journal of Catalysis*, 2023, **54**, 290-297.
13. M. Zhong, N. Song, C. Li, C. Wang, W. Chen and X. Lu, *Journal of Colloid and Interface Science*, 2022, **614**, 556-565.
14. S. L. Fereja, P. Li, Z. Zhang, J. Guo, Z. Fang, Z. Li and W. Chen, *Electrochimica Acta*, 2022, **405**, 139793.
15. L. Wang, P. Wang, X. Xue, D. Wang, H. Shang, Y. Zhao and B. Zhang, *Journal of Colloid and Interface Science*, 2024, **665**, 88-99.
16. A. Meena, P. Thangavel, D. S. Jeong, A. N. Singh, A. Jana, H. Im, D. A. Nguyen and K. S. Kim, *Applied Catalysis B: Environmental*, 2022, **306**, 121127.
17. N. K. Shrestha, S. A. Patil, J. Han, S. Cho, A. I. Inamdar, H. Kim and H. Im, *Journal of Materials Chemistry A*, 2022, **10**, 8989-9000.
18. A. Kumar, J. Muhommad, S. K. Purkayastha, A. K. Guha, M. R. Das and S. Deka, *ACS Sustainable Chemistry & Engineering*, 2023, **11**, 2541-2553.
19. W. Yang, Q. Zhang, S. S. Siwal, Y. Hua and C. Xu, *Electrochimica Acta*, 2020, **361**, 137038.
20. N. Cheng, Q. Liu, A. M. Asiri, W. Xing and X. Sun, *Journal of Materials Chemistry A*, 2015, **3**, 23207-23212.
21. Y. Wu, Y. Liu, B. Liu, W. Jiang, T. Zhou, H. Li, M. Shang, J. Lang, C. Liu and G. Che, *ACS Applied Nano Materials*, 2022, **5**, 7714-7722.
22. Y. Huang, Y. Wu, Z. Zhang, L. Yang and Q. Zang, *Electrochimica Acta*, 2021, **390**, 138754.
23. X. Zhang, Y. Qiu, W. Zhang, X. Ji and J. Liu, *Sustainable Energy & Fuels*, 2021,

5, 2228-2233.
24. H. Zhang, G. Qian, T. Yu, J. Chen, L. Luo and S. Yin, *ACS Sustainable Chemistry & Engineering*, 2021, **9**, 8249-8256.
25. Z. Wang, S. Liu, J. Du, Y. Xing, Y. Hu, Y. Ma, X. Lu and C. Wang, *Green Chemistry*, 2024, **26**, 7779-7788.